Comparisons of Frequency Response Function Identification Methods using Single Motion Data: Time- and Frequency-domain Approaches

Hiroki Tachibana
Department of Electrical and Mechanical Engineering
Nagoya Institute of Technology
Nagoya, Japan
Email: h.tachibana.776@stn.nitech.ac.jp

Naoki Tanaka
Department of Electrical and Electronic Engineering
Nagoya Institute of Technology
Nagoya, Japan
Email: n.tanaka.933@stn.nitech.ac.jp

Yoshihiro Maeda
Department of Electrical and Mechanical Engineering
Nagoya Institute of Technology
Nagoya, Japan
Email: ymaeda@nitech.ac.jp

Makoto Iwasaki
Department of Electrical and Mechanical Engineering
Nagoya Institute of Technology
Nagoya, Japan
Email: iwasaki@nitech.ac.jp

Abstract—In this paper, frequency response function (FRF) identification methods using single point-to-point motion data for the fast and precise motion control of industrial servo systems are examined. The adaptation of controllers using an identified FRF is effective for maintaining the motion accuracy, even if plant parameters vary in the processing operation. However, it is difficult to achieve an accurate FRF from the motion data during repetitive motions with short time-intervals. In this study, a time-domain least squares method-based FRF identification method and a frequency-domain discrete Fourier transform-based FRF identification method were theoretically and experimentally evaluated, using a laboratory galvano scanner.

Index Terms—frequency response function identification, discrete Fourier transform, least squares method, one-shot motion, fast and precise positioning

I. INTRODUCTION

Regarding the demands of high-throughput in industrial mechatronic systems such as electronics processing machines, the fast and precise point-to-point (PTP) positioning motion is repetitively performed (so-called "inching motion") with short time intervals (the time interval is defined as a period between the start of the previous motion and the start of the next motion) [1], [2]. As an example, in a high density interconnected (HDI) printed circuit board (PCB) laser drilling machine, galvano scanners for positioning the laser beam to desired positions on PCBs perform numerous PTP motions with short time intervals. In the fast and short time interval motion, since parameters of a galvano scanner such as torque constant and resonant frequencies vary owing to environmental temperature and self-heating, overshoot and/or vibratory responses often deteriorate the positioning accuracy [3], [4].

To solve the above problem, the adaptive feedforward (FF) compensation based on a frequency response function (FRF) of a target system is a promising approach [2], and varieties of

FRF identification methods that are suitable for the adaptive compensation have been studied in related research fields [5]–[8]. In recent years, FRF identification methods using single PTP motion data [9]–[11] have been actively studied. The FRF identification methods do not require stopping the processing operation of industrial systems [10], although the widely-used sine sweep methods require the processing operation to stop for a while. The most widespread FRF identification method using one-shot PTP motion data is the least squares method (LSM)-based method using a high-order Auto Regressive with eXogenous (ARX) model [8], [11], [12]. The LSM-based FRF identification method efficiently estimates the ARX model parameters based on an optimization problem in time-domain and identifies an FRF. However, it is well-known that the identification accuracy in the frequency-domain is not satisfactory since the LSM-based method is a time-domain approach [12].

On the other hand, frequency-domain FRF identification methods using single PTP motion data [10], [13] have been studied to achieve a more accurate FRF than the time-domain FRF identification methods. The frequency-domain FRF identification methods simply depend on the discrete Fourier transform (DFT) of input and output data during a single PTP motion, and directly identifies an FRF of a target system in the frequency-domain. In [13], three frequency-domain FRF identification methods using different pre-filters have been comparatively evaluated, especially focusing on the effects of the time interval of the repetitive motion.

In this paper, a time-domain LSM-based FRF identification method [12] and a frequency-domain DFT-based FRF identification method proposed by the authors in [13] are comparatively evaluated (theoretically and experimentally) to determine a suitable method for identifying an accurate FRF

Fig. 1. External appearance of a laboratory galvano scanner.

Fig. 2. Bode characteristics of a galvano scanner measured by a sine sweep experiment.

Fig. 3. Experimental response waveforms of position and position error in short-interval repetitive motion.
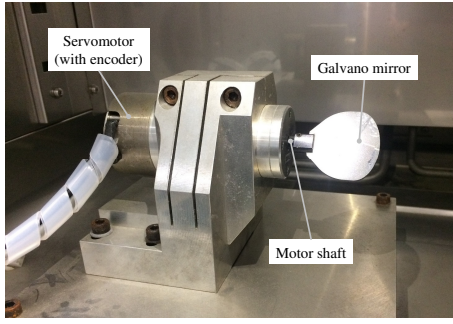
for the adaptive compensation. Theoretical features of the two FRF identification methods were described in detail. In addition, FRF identification experiments using a laboratory galvano scanner were performed, focusing on the robustness against a change of the time interval.

II. GALVANO SCANNER AND CONTROL SYSTEM

A. Galvano Scanner

The external appearance of a laboratory galvano scanner for laser drilling of PCBs is shown in Fig. 1. A DC servomotor rotates a galvano mirror mounted on the motor shaft and a rotary encoder detects motor angle θ_m with resolution of 1.49×10^{-6} rad. The servo controller (sampling time of $T_s = 20$ μs) outputs a motor current reference i_{ref} as a control input to a servo amplifier. To realize high-throughput PCB processing with high-quality, the fast and precise motion control of a galvano scanner is one of the primary technologies.

Black dotted lines in Fig. 2 show a bode plot of θ_m for i_{ref} measured via a sine sweep experiment using a servo analyzer (Ono sokki, DS3000). The galvano scanner contains the first resonant mode at 2.9 kHz and the second resonant mode at 6.3 kHz that are generated by deformation of the galvano mirror and torsion of the motor shaft. A plant model $P(s) = \theta_m(s)/i_{ref}(s)$ focusing on the experimental gain characteristic is formulated by (1) as a summation of a rigid mode and two resonant modes:

$$P(s) = K_g \left(\frac{1}{s^2} + \sum_{l=1}^{2} \frac{k_l}{s^2 + 2\zeta_l \omega_l s + \omega_l^2} \right) \quad (1)$$

where K_g is the gain considering the moment of inertia J and torque constant of motor K_t, ω_l is the natural angular frequency of l-th resonant mode, ζ_l is the damping coefficient, and k_l is the resonant mode gain, respectively.

B. Target Control Specification

In industrial PCB processing machines, a galvano scanner performs numerous PTP positioning motions with short time intervals to make via holes on PCBs in short tact time [8], [11]. Fig. 3 shows an example of experimental response waveforms of the position and the position error with the target position stroke of $X_r = 1$ mm (in laser position) and the interval time of 0.76 ms (the shortest time interval). As
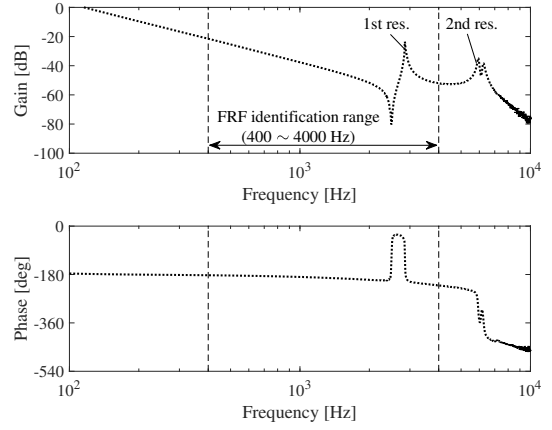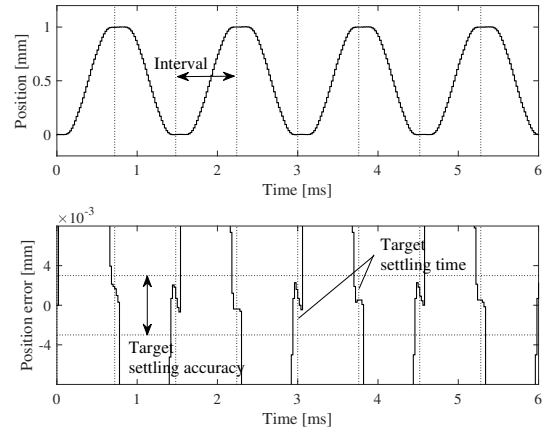
a target control specification, each position response should settle to the target position within the target settling accuracy of ± 3 μm (horizontal dotted lines) by the settling time of 0.72 ms (vertical dotted lines).

Here, note that the torque constant K_t and the resonant frequencies ω_1 and ω_2 vary depending on environmental temperature and self-heating in the PCB processing operation [8]. In particular, variations of K_t and ω_1 notably deteriorates the positioning accuracy. Therefore, an adaptive compensation strategy is required to maintain the fast and precise control performance. In addition, to realize that, fast and accurate identification of an FRF of a galvano scanner in a frequency range of $400 \sim 4000$ Hz is required during the short-interval PTP motions as shown in Fig. 3.

C. Adaptive PTP Position Control System

Fig. 4 depicts a block diagram of the two-degree-of-freedom (2DoF) position control system for the galvano scanner, where $C(z)$ is the feedback (FB) controller composed of a PID compensator and two second-order resonance compensation filters according to [14], $P_n(z)$ is the discrete-time plant model considering $P(s)$ of (1) and a phase delay model (ε^{-Ls}),
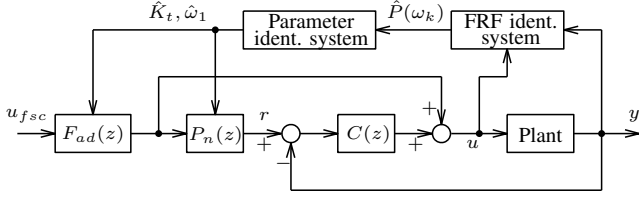
Fig. 4. Block diagram of adaptive 2DoF position control system.

$F_{ad}(z)$ is the adaptation filter, u_{fsc} is the FF control input generated by the final-state control (FSC) framework [3], $u(= i_{ref})$ is the control input, r is the target position trajectory reference, and $y(\propto \theta_m)$ is the motor position, respectively. The FSC-based FF control is designed so that y settles to the target position X_r by 0.72 ms. To achieve fine adaptive control performance, an accurate FRF $\hat{P}(\omega_k)$ from the single PTP motion data u and y as shown in Fig. 5 are required for adapting $F_{ad}(z)$ and $P_n(z)$ with accurate $\hat{K}_t$ and $\hat{\omega}_1$.

III. FRF IDENTIFICATION METHODS USING SINGLE MOTION DATA

In this section, the time-domain LSM-based FRF identification method [12] and the frequency-domain DFT-based FRF identification method proposed by the authors in [13] are briefly introduced and their theoretical features are explained.

A. Least Squares Method-based FRF Identification [12]

Fig. 6 shows a block diagram of a the LSM-based FRF identification system for the discretized plant system $P(z)$. The input and output data $\{u_i, y_i\}$ at $t = iT_s$ $(i = 0, \ldots, N-1)$ of a single PTP motion (i.e., the time interval is NT_s) are available for FRF identification. In this system, first, the parameters of an estimated plant model $\hat{P}(z)$ are identified via the LSM in time-domain, and then, an FRF $\hat{P}(\omega_k)$ $(k = 0, 1, \ldots, M-1)$ is calculated based on the discrete-time Fourier transform.

The actual plant $P(z)$ is defined by (2) as an N_p-th order ARX model:

$$
\begin{aligned}
P(z) &= \frac{B(z)}{A(z)} \\
A(z) &= 1 + a_1 z^{-1} + \cdots + a_{N_p} z^{-N_p} \\
B(z) &= b_1 z^{-1} + \cdots + b_{N_p} z^{-N_p}
\end{aligned}
\tag{2}
$$

where $a_n \in \mathbb{R}$ and $b_n \in \mathbb{R}$ $(n = 1, \ldots, N_p)$ are the plant parameters required to be identified. By considering (2), the output data y_i in the sample time-domain is expressed as

$$
\begin{aligned}
y_i &= -a_1 y_{i-1} - a_2 y_{i-2} \cdots - a_{N_p} y_{i-N_p} \\
&\quad + b_1 u_{i-1} + b_2 u_{i-2} \cdots + b_{N_p} u_{i-N_p} \\
&= \boldsymbol{\theta}^T \boldsymbol{\phi}_i
\end{aligned}
\tag{3}
$$

where the unknown parameter vector $\boldsymbol{\theta} \in \mathbb{R}^{2N_p}$ and the data vector $\boldsymbol{\phi}_i \in \mathbb{R}^{2N_p}$ are defined as follows:

$$
\begin{aligned}
\boldsymbol{\theta} &= [-a_1 \ -a_2 \ \cdots \ -a_{N_p} \ b_1 \ b_2 \ \cdots \ b_{N_p}]^T \\
\boldsymbol{\phi}_i &= [y_{i-1} \ y_{i-2} \ \cdots \ y_{i-N_p} \ u_{i-1} \ u_{i-2} \ \cdots \ u_{i-N_p}]^T.
\end{aligned}
\tag{4}
$$
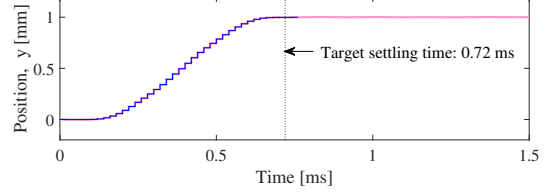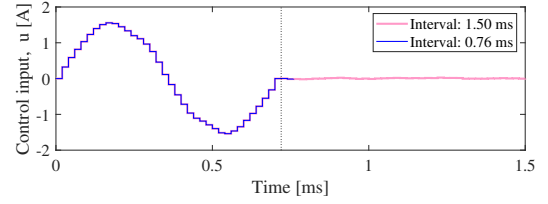
Fig. 5. Single PTP motion data of control input and position.
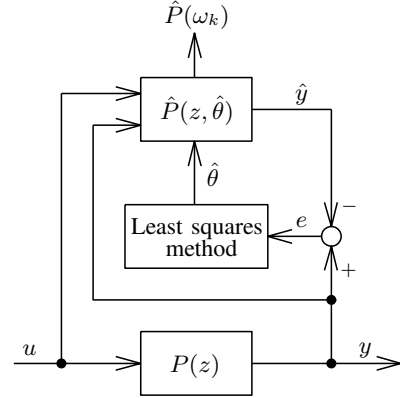
Fig. 6. Time-domain FRF identification system based on the least sqares method (LSM).

The estimated parameters $\hat{\boldsymbol{\theta}}$ are obtained by minimizing the following quadratic objective function.

$$
J = \sum_{i=0}^{N-1} e_i^2 = \sum_{i=0}^{N-1} \left(y_i - \hat{y}_i(\hat{\boldsymbol{\theta}}) \right)^2
\tag{5}
$$

where the estimated output $\hat{y}(z, \hat{\boldsymbol{\theta}})$ is defined by

$$
\hat{y}(z, \hat{\boldsymbol{\theta}}) = \{1 - A(z, \hat{\boldsymbol{\theta}})\} y(z) + B(z, \hat{\boldsymbol{\theta}}) u(z).
\tag{6}
$$

The optimum $\hat{\boldsymbol{\theta}}$ is estimated as (7) considering $\partial J / \partial \hat{\boldsymbol{\theta}} = 0$.

$$
\hat{\boldsymbol{\theta}} = \left(\sum_{i=0}^{N-1} \boldsymbol{\phi}_i \boldsymbol{\phi}_i^T \right)^{-1} \left(\sum_{i=0}^{N-1} \boldsymbol{\phi}_i y_i \right)
\tag{7}
$$

Finally, the identified FRF $\hat{P}(\omega_k)$ at frequencies ω_k is obtained from $\hat{P}(z, \hat{\boldsymbol{\theta}})$, by substituting $z = \varepsilon^{j\omega_k T_s}$.

Here, a frequency-domain objective function corresponding to the time-domain objective function of (5) is defined as follows, based on the Parseval's theorem:

$$
J = \sum_{i=0}^{N-1} e_i^2 = \frac{1}{N} \sum_{k=0}^{N-1} E(\omega_k)^2
\tag{8}
$$
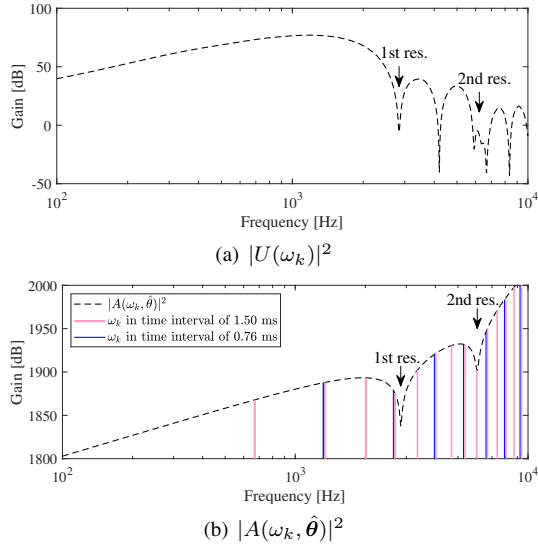
(a) $|U(\omega_k)|^2$

(b) $|A(\omega_k, \hat{\boldsymbol{\theta}})|^2$

Fig. 7. Gain characteristics of weighting functions: (a) $|U(\omega_k)|^2$; (b) $|A(\omega_k, \hat{\boldsymbol{\theta}})|^2$ under $\hat{\boldsymbol{\theta}} = \boldsymbol{\theta}$.

where $E(\omega_k)$ is the DFT of e_i at a frequency of $\omega_k = \frac{2\pi k}{N T_s}$ and is expressed as

$$E(\omega_k) = A(\omega_k, \hat{\boldsymbol{\theta}}) \left(Y(\omega_k) - \frac{B(\omega_k, \hat{\boldsymbol{\theta}})}{A(\omega_k, \hat{\boldsymbol{\theta}})} U(\omega_k) \right). \quad (9)$$

Therefore, the frequency-domain objective function can be expressed as

$$J = \frac{1}{N} \sum_{k=0}^{N-1} |A(\omega_k, \hat{\boldsymbol{\theta}})|^2 |U(\omega_k)|^2 |P(\omega_k) - \hat{P}(\omega_k, \hat{\boldsymbol{\theta}})|^2. \quad (10)$$

From (10), the LSM-based FRF identification includes frequency-domain weighting functions $|U(\omega_k)|^2$ and $|A(\omega_k, \hat{\boldsymbol{\theta}})|^2$ in theory. In general, since $|A(\omega_k, \hat{\boldsymbol{\theta}})|^2$ has higher gains in a high frequency range as shown by a black broken line in Fig. 7(b), the LSM-based FRF identification method tends to optimize the higher frequency range [12] even though $|U(\omega_k)|^2$ is generally small in the high frequency range, as shown in Fig. 7(a). Therefore, the LSM-based FRF identification method might experience difficulty in achieving an accurate FRF in a low frequency range.

B. DFT-based FRF Identification Method [13]

A block diagram of the DFT-based FRF identification system is shown in Fig. 8, where $\hat{P}(\omega_k)$ is the identified FRF, $F(z)$ is the pre-filter, which is explained later, u_f is the filtered input, y_f is the filtered output, $U_f(\omega_k)$ is the DFT of u_f, and $Y_f(\omega_k)$ is the DFT of y_f. In this system, first, the single motion data $\{u_i, y_i\}$ at $t = iT_s$ $(i = 0, \ldots, N-1)$ are input to $F(z)$, and $F(z)$ calculates the output data $\{u_{fi}, y_{fi}\}$ on-line. Second, $\{u_{fi}, y_{fi}\}$ is transferred to the DFT algorithm, where the DFT data length is $M(\geq N)$, i.e., $\boldsymbol{u}_f = [u_{f0}, u_{f1}, \ldots, u_{f(N-1)}, 0, \ldots, 0]^T \in \mathbb{R}^M$ and $\boldsymbol{y}_f = [y_{f0}, y_{f1}, \ldots, y_{f(N-1)}, 0, \ldots, 0]^T \in \mathbb{R}^M$. Finally, using the DFT results $U_f(\omega_k)$ and $Y_f(\omega_k)$ $(k = 0, 1, \ldots, M-1)$
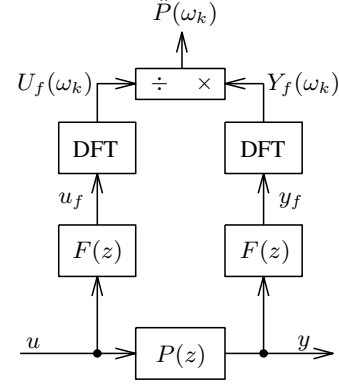
Fig. 8. Frequency-domain FRF identification system based on the DFT.
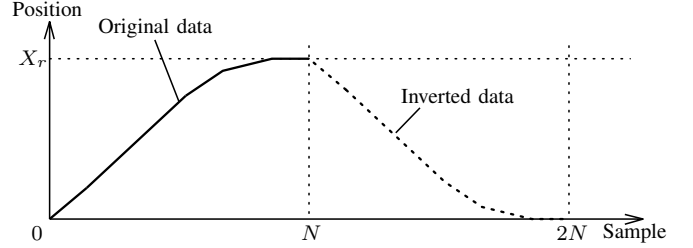
Fig. 9. Conceptual diagram of single PTP motion data in the DFT-based FRF identification method using a differentiator.

of $\boldsymbol{u}_f$ and $\boldsymbol{y}_f$, the identified FRF $\hat{P}(\omega_k) = Y_f(\omega_k)/U_f(\omega_k)$ is obtained. The parameter estimation of an ARX model $\hat{P}(z)$ as in III-A is not required.

In general, the time-domain data u_i and y_i in a single PTP motion are not cyclic (i.e., $u_0 \neq u_{N-1}$ or $y_0 \neq y_{N-1}$) as shown in Fig. 5, which results in undesired frequency components on the DFT results [9], [10]. In [13], the differentiator-based pre-filter of (11) is used to make u_i and y_i cyclic.

$$F(z) = 1 - z^{-1} \quad (11)$$

To explain the theoretical meaning of introducing (11) as $F(z)$, a concept of the DFT-based FRF identification method using the differentiator is shown in Fig. 9. A solid line represents an example of single PTP motion data of position as an original data $y_{oi} = y_i (i = 0, \ldots, N-1)$. To obtain a cyclic data with data length of $2N$, y_{oi} and its inverted data $y_{o(N-1)} - y_{o(i+N)}$ with N steps shifted are connected as indicated by a dotted line. Using y_{oi}, the connected signal y_{cm} $(m = 0, \ldots, 2N-1)$ is expressed as

$$y_{cm} = \begin{cases} y_{om} & : m = 0, \ldots, N-1 \\ y_{o(N-1)} - y_{o(m-N)} \\ \quad : m = N, \ldots, 2N-1 \end{cases} . \quad (12)$$

The DFT $Y_c(\omega_k)$ of (12) is expressed as

$$Y_c(\omega_k) = \sum_{m=0}^{2N-1} y_{cm} \varepsilon^{-jm\omega_k T_s} \quad (13)$$

where the discrete frequency of ω_k is defined as $\omega_k = \frac{2\pi k}{2NT_s}$. Equation (13) can be reformulated as (14), considering the differential data y'_{cm} of y_{cm}.

$$Y_c(\omega_k) = y'_{c0} + (y'_{c0} + y'_{c1})\varepsilon^{-j\omega_k T_s} + \cdots$$
$$+ \sum_{m=0}^{2N-1} y'_{cm}\varepsilon^{-j(2N-1)\omega_k T_s}, \quad (14)$$

$$y'_{cm} = y_{cm} - y_{c(m-1)}, \quad y_{c(-1)} = 0.$$

Here, y'_c satisfies the following equation from (12).

$$y'_{ci} = -y'_{c(i+N)} \quad (i = 0, \ldots, N-1) \quad (15)$$

Considering (14) and (15), $Y_c(\omega_k)$ is reformulated as follows:

$$Y_c(\omega_k) = y'_{c0} \sum_{i=0}^{N-1} \varepsilon^{-ji\omega_k T_s} + y'_{c1} \sum_{i=0}^{N-1} \varepsilon^{-ji\omega_k T_s} + \cdots$$

$$+ y'_{c(N-1)} \sum_{i=0}^{N-1} \varepsilon^{-ji\omega_k T_s} \quad (16)$$

$$= \sum_{i=0}^{N-1} y'_{ci}\varepsilon^{-ji\omega_k T_s} \cdot \sum_{i=0}^{N-1} \varepsilon^{-ji\omega_k T_s}.$$

As a result, the identified FRF $\hat{P}(\omega_k)$ calculated from u_{cm} and y_{cm} has the following relationship:

$$\hat{P}(\omega_k) = \frac{\sum_{i=0}^{N-1} y'_{ci}\varepsilon^{-ji\omega_k T_s}}{\sum_{i=0}^{N-1} u'_{ci}\varepsilon^{-ji\omega_k T_s}} = \frac{Y'_o(\omega_k)}{U'_o(\omega_k)} = \frac{Y_c(\omega_k)}{U_c(\omega_k)}. \quad (17)$$

Notice that, introducing the differentiator of (11), the concept of Fig. 9 can be equivalently realized. For more detailed explanation regarding the DFT-based FRF identification method and comparative evaluations with other frequency-domain FRF identification methods, refer [13].

IV. EVALUATIONS OF TIME- AND FREQUENCY-DOMAIN FRF IDENTIFICATION METHODS

A. Experimental Setup

Fig. 10 shows a configuration of a laboratory experimental setup. The 2DoF position control system (without the adaptation of the FF compensation) explained in II-C and the FRF identification systems introduced in III-A and III-B were implemented on a DSP (System Design Service, Ltd, PDRS-6000). The FRF of the galvano scanner was identified using single PTP motion data of u and y. To evaluate the robustness against variations of the time interval, the PTP motion data shown in Fig. 5 with the time intervals of 1.50 ms and 0.76 ms were used for the FRF identification.

In the LSM-based FRF identification method, the ARX model $\hat{P}(z)$ defined by (18) with the order of $N_p = 20$, which is higher than the one of (1), was used considering the effects of quantization errors, unknown modeling errors, and noise at high frequencies [11], [12].

$$\hat{P}(z) = \frac{b_1 z^{-1} + \cdots + b_{20} z^{-20}}{1 + a_1 z^{-1} + \cdots + a_{20} z^{-20}}. \quad (18)$$

On the other hand, in the DFT-based FRF identification method, the data length M of the DFT was determined as
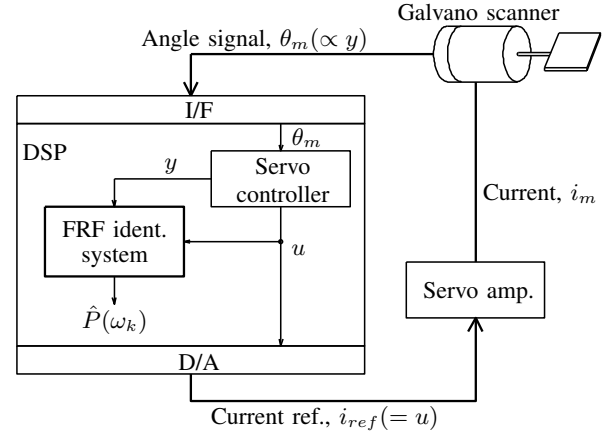
Fig. 10. Configuration of experimental setup for FRF identification.

$M = 5000$ to ensure sufficient frequency resolution for the FRF identification. Note that, in both the FRF identification methods, the FRFs $\hat{P}(\omega_k)$ were calculated at the same discrete frequency ω_k.

B. Experimental Results of FRF Identification

The FRF identification results of the LSM-based and the DFT-based methods in the time intervals of 1.50 ms ($N = 75$) and 0.76 ms ($N = 38$) are shown in Fig. 11, while the identification errors defined by $|P(\omega_k) - \hat{P}(\omega_k)|$ are shown in Fig. 12. Note that the evaluation frequency range was selected at $400 \sim 4000$ Hz and the FRF measured by the sine sweep experiment shown in Fig. 2 was defined as a reference FRF $P(\omega_k)$ of the galvano scanner in the following evaluations. In Fig. 11 and Fig. 12, black dotted lines are the results of the sine sweep experiment (same as in Fig. 2), red solid lines are the ones of the LSM-based method (LSM), and blue solid lines are the ones of the differentiator-based method (DIF), respectively.

In the longer interval of 1.50 ms, the LSM-based FRF identification method could accurately identify not only the rigid mode in the low frequency range below 1 kHz but also the first resonant mode. However, in the shorter interval of 0.76 ms, significant identification errors were recognized. Here, red solid lines and blue solid lines in Fig. 7 show the evaluation frequencies ω_k in the time intervals of 1.50 ms and 0.76 ms. From the figure, the number of ω_k in the low frequency range decreases in the shorter interval motion, owing to the frequency resolution $\Delta\omega = \omega_k - \omega_{k-1} = \frac{2\pi}{NT_s}$ in the DFT ($\Delta\omega = 2\pi \times 667$ rad/s in the time interval of 1.50 ms and $\Delta\omega = 2\pi \times 1316$ rad/s in the time interval of 0.76 ms). Therefore, the FRF identification errors in the shorter interval motion is considered as the effects of the weighting function $|A(\omega_k, \hat{\boldsymbol{\theta}})|^2$ in the LSM as elucidated in III-A.

On the other hand, the proposed DFT-based FRF identification method successfully reproduced $P(\omega_k)$ in both cases. The variations of the FRF identification results were explicitly small, as shown in Fig. 12, compared to the ones of the LSM-based FRF identification method.

(a) Interval: 1.50 ms   (b) Interval: 0.76 ms
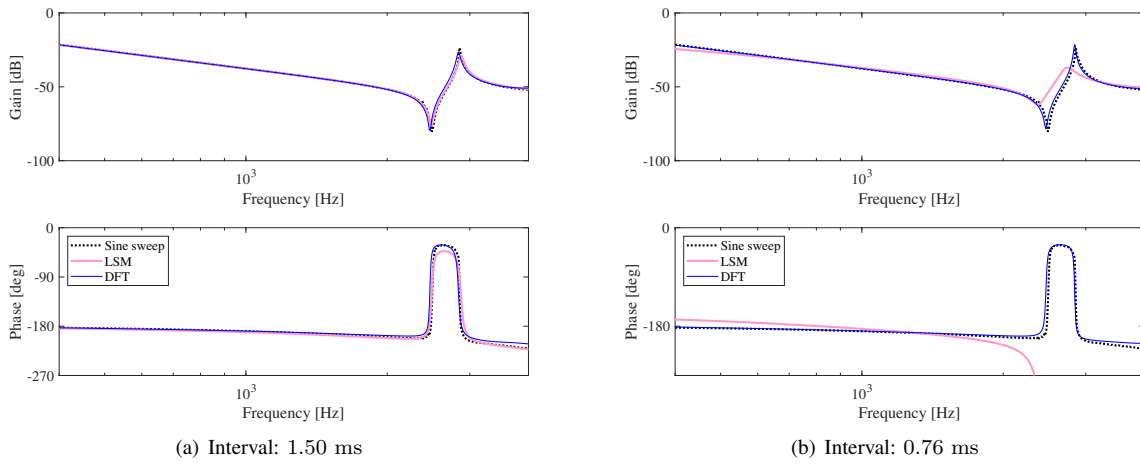
Fig. 11. Comparisons of FRF identification results for one-shot PTP motion data: (a) time interval of 1.50 ms; (b) time interval of 0.76 ms.
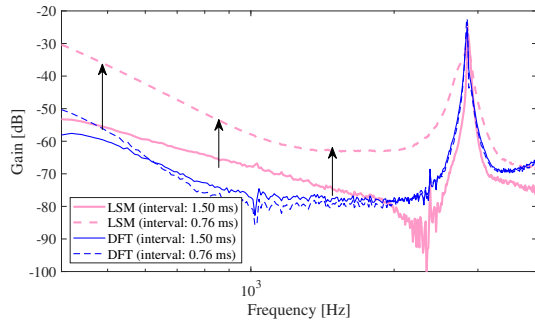
Fig. 12. Comparisons of FRF identification errors, $|P(\omega_k) - \hat{P}(\omega_k)|$.

V. CONCLUSION

In this paper, time- and frequency-domain FRF identification methods using single PTP motion data (the LSM-based method and the DFT-based method proposed by the authors in [13]) were comparatively evaluated, for adaptive, fast, precise, and short time interval positioning control. In the LSM-based FRF identification method, since the frequency-domain objective function of the LSM theoretically possessed low weights in a lower frequency range, the identified FRF included remarkable identification errors, especially in the short interval motion. On the other hand, the DFT-based FRF identification method using the differentiator-based pre-filtering could obtain an accurate FRF, even in the short interval motion. From the series of experimental evaluations using a laboratory galvano scanner, it has been determined that the proposed frequency-domain DFT-based FRF identification method would be more suitable for performing the adaptive compensation in the PCB processing operation.

As a future work, the adaptive FF compensation with the proposed DFT-based FRF identification method will be evaluated through experiments.

ACKNOWLEDGMENT

REFERENCES

[1] M.-Y. Chen and J.-S. Lu, "High-precision motion control for a linear permanent magnet iron core synchronous motor drive in position platform," *IEEE Trans. Ind. Informat.*, vol. 10, no. 1, pp. 99–108, 2014.

[2] Y. Maeda and M. Iwasaki, "Feedforward friction compensation using rolling friction model for micrometer-stroke point-to-point positioning motion," *IEEJ J. Industry Applications*, vol. 7, no. 2, pp. 141-149, 2018.

[3] S. Ueda and M. Hirata, "Final-state control for a galvano scanner: minimizing mirror vibration in an inclined direction relative to the rotation axis," in *IEEE Conf. Decision and Control*, pp. 3289-3294, 2017.

[4] Y. Maeda and M. Iwasaki, "Improvement of adaptive property by adaptive deadbeat feedforward compensation without convex optimization," *IEEE Trans. Ind. Electron.*, vol. 62, no. 1, pp. 466–474, 2015.

[5] R. Voorhoeve, A. van der Maas, and T. Oomen, "Non-parametric identification of multivariable systems: A local rational modeling approach with application to a vibration isolation benchmark," *Mechanical Systems and Signal Processing*, vol. 105, pp. 129–152, 2018.

[6] Y.-Y. Chen, P.-Y. Huang, and J.-Y. Yen, "Frequency-domain identification algorithms for servo systems with friction," *IEEE Trans. Control Syst. Tech.*, vol. 10, no. 5, pp. 654–665, 2002.

[7] C.K. Pang and F.L. Lewis, "System identification of modal parameters in dual-stage Hard Disk Drives," in *Proc. 2009 IEEE Int. Conf. Control and Automation*, pp. 603–608, 2018.

[8] Y. Maeda, K. Harata, and M. Iwasaki, "A friction model-based frequency response analysis for frictional servo systems," *IEEE Trans. Ind. Informat.*, vol. 14, no. 11, pp. 5246–5255, 2018.

[9] Y. Matsui, H. Ayano, and K. Nakano, "Parametric plant modeling using one-shot closed-loop transient response data," in *Proc. 11th Int. Conf. Electrical Eng./Electronics, Computer, Telecommunications and Information Technology*, pp. 1–6, 2014.

[10] Y. Matsui, T. Kimura, and K. Nakano, "Plant model analysis based on closed-loop step response data," in *Proc. IEEE Int. Conf. Control Applications*, pp. 677–682, 2010.

[11] H. Sekine, S. Ueda, and M. Hirata, "System identification of a galvano scanner using input-output data obtained from positioning control," in *Proc. 2015 European Control Conf.*, pp. 1297–1302, 2015.

[12] S. Hashimoto, S. Adachi, and H. Funato, "Derivation of modal parameters of a flexible structure based on the multi-decimation identification method," in *Proc. 2002 IEEE Int. Symposium Ind. Electron.*, pp. 436–440, 2002.

[13] Y. Maeda, H. Tachibana, and M. Iwasaki, "Comparative evaluations of frequency response analysis methods for fast and precise point-to-point position control," in *Proc. 15th IEEE Int. Workshop Adv. Motion Control*, pp. 437–442, 2018.

[14] Y. Maeda, E. Kuroda, T. Uchizono, and M. Iwasaki, "Hybrid optimization method for high-performance cascade structure feedback controller design," in *Proc. 44th Annu. Conf. IEEE Ind. Electron. Society*, pp. 4588–4593, 2018.